Multistep Denaturation of *Borrelia burgdorferi* OspA, a Protein Containing a Single-Layer β-Sheet[†]

Shohei Koide,*[,‡] Zimei Bu,[§] Dipesh Risal,[‡] Thúy-Nga Pham,[‡] Tomoko Nakagawa,[||] Atsuo Tamura,[||] and Donald M. Engelman[§]

Department of Biochemistry and Biophysics, University of Rochester Medical Center, Rochester, New York 14642, Department of Molecular Biophysics and Biochemistry, Yale University, New Haven, Connecticut 06511, and Graduate School of Science and Technology, Kobe University, Kobe 657-8501, Japan

Received October 14, 1998

ABSTRACT: Outer surface protein A (OspA) from the Lyme disease spirochete, *Borrelia burgdorferi*, is a dumbbell-shaped protein in which two globular domains are connected by a three-stranded β-sheet segment that is solvent-exposed on both faces. Previous studies showed that the whole protein, including the single-layer β-sheet, is highly rigid. To elucidate the folding mechanism and the role of the central β-sheet in the formation of the rigid molecule, we investigated the equilibrium thermal denaturation reaction of OspA. We applied differential scanning calorimetry, heteronuclear NMR spectroscopy, and solution small-angle X-ray scattering (SAXS) to characterize the reaction in detail. All three techniques revealed that OspA denatures in two separable cooperative transitions. NMR measurements on OspA specifically ^{15}N-labeled at Lys residues identified the locations of the two folding units and revealed that the C-terminal segment is less stable than the remaining N-terminal segment. The boundary between the two folding units is located within the central β-sheet. The interconversion among the three folding states (fully folded, C-terminus unfolded, and fully denatured) is slow relative to chemical shift differences ($<$24 Hz), indicating that there are significant kinetic barriers in the denaturation reactions. SAXS measurements determined the radius of gyration of the native protein to be 25.0 $\pm$ 0.3 Å, which increases to 34.4 $\pm$ 1.0 Å in the first transition, and then to 56.1 $\pm$ 1.6 Å in the second transition. Thus, the intermediate state, in which the C-terminal folding unit is already denatured, is still compact. These results provide a basis for elucidating the folding mechanism of OspA.

The folded conformation of a protein is stabilized by different factors including the hydrophobic effect, hydrogen bonding, packing, and electrostatic interactions. Studies from a variety of soluble proteins have established that the formation of a hydrophobic core that removes hydrophobic surface from contact with water is a major force for protein folding (*1*−*3*). It is still challenging to quantify contributions of these factors to the stabilization of a unique conformation. A unique protein structure can be specifically stabilized by positive design, that is, by reducing the free energy of the particular structure, or by negative design, that is, by increasing the free energy of alternative conformations, such as denatured states.

Outer surface protein A (OspA)[1] from the Lyme disease spirochete *Borrelia burgdorferi* is a 31 kDa abundant antigenic lipoprotein. The crystal structure of a soluble form of OspA (hereafter referred to simply as OspA) complexed with the Fab fragment of a monoclonal antibody revealed a highly unusual structure of this protein (*4*). OspA consists of 21 consecutive antiparallel β-strands and a C-terminal α-helix. It contains a unique single-layer β-sheet which connects the N- and C-terminal globular domains (in this article we use the terms N- and C-terminal domains and central β-sheet for clarity, but we do not wish to imply that they correspond to independent folding units). Such a single-layer β-sheet is unique among known protein structures.

Nuclear magnetic resonance (NMR) spectroscopy and solution small-angle X-ray scattering (SAXS) analyses have demonstrated that the solution conformation of OspA in the absence of the bound antibody fragment is close to its crystal structure (*5*, *6*). Further, amide H−D exchange measurements have demonstrated that the central β-sheet is highly stable, despite the fact that it is solvent-exposed on both faces (*7*). On the basis of an analysis of the crystal structure, Pham et al. found that an increased thickness of the central β-sheet buries nonpolar surface to a degree comparable to those found in small globular proteins, suggesting that the hydrophobic effect is the dominant stabilizing force (*7*). They also proposed that characteristic cross-strand Glu-Lys pairs may play an important role in defining this particular conformation via negative design.

[†] This work was supported in part by an NIH Grant GM-22778 to D.M.E. and by a Grant-in-Aid for Scientific Research from the Ministry of Education, Science, Sports, and Culture of Japan to A.T.

* To whom correspondence should be addressed. Fax: (716) 275−6007. E-mail: Shohei_Koide@urmc.rochester.edu.

[‡] University of Rochester Medical Center.

[§] Yale University.

[||] Kobe University.

[1] Abbreviations: CD, circular dichroism; DSC, differential scanning calorimetry; GuHCl, guanidine hydrochloride; HSQC, heteronuclear single-quantum correlation; NMR, nuclear magnetic resonance; OspA, outer surface protein A; Rg, radius of gyration; SAXS, small-angle X-ray scattering; SVD, singular value decomposition.

10.1021/bi982443+ CCC: $18.00
Published on Web 03/26/1999

Most β-sheets observed in protein structures are amphipathic, and usually the hydrophobic face of these β-sheets is involved in extensive contacts through a hydrophobic core. These contacts makes it difficult to dissect contributions of local and nonlocal interactions. Previous studies using globular proteins have shown that amino acids have distinct β-sheet-forming propensities, but these propensities are somewhat dependent on structural context (*8*−*12*). Thus, the OspA central β-sheet may provide a unique opportunity to investigate the energetics and folding of β-sheets in the absence of long-range interactions. Studies of OspA may also help identify important factors in the energetics of proteins which are not evident in the conventional form of β-sheet. In addition, the OspA central β-sheet may be a good starting point for engineering small β-sheet-forming peptides (*13*).

OspA is also a promising candidate for a Lyme disease vaccine. It has been shown that OspA can elicit protective immunity against the *Borrelia* infection in mice (*14*). Protective anti-OspA antibodies bind C-terminal regions in the folded form of OspA (*15*, *16*). Knowledge of the stability and folding mechanism of OspA could be useful for designing a recombinant vaccine based on OspA fragments.

To gain insights into the energetics and folding of this unique protein, we undertook equilibrium unfolding studies of OspA. The amide H−D exchange study (*7*) showed that the N-terminal domain (strands 1−7) and the first strand (strand 8) of the central β-sheet contain residues that are most protected. Strands 9−11 contain residues that exhibit intermediate protection, and the C-terminal domain (strands 12−the C-terminus) shows the least protection. These results suggest that, in an equilibrium unfolding experiment, the C-terminal domain might unfold first, followed by the central segment, and then by the N-terminal domain. However, one should be cautious about interpreting amide H−D exchange data. For example, amide protons in a small globular protein show a range of protection, but such a protein often unfolds in a single cooperative transition.

In this study, we observed the temperature-induced equilibrium unfolding of OspA using differential scanning calorimetry (DSC), heteronuclear NMR spectroscopy, and solution SAXS. DSC and NMR experiments clearly demonstrated that OspA undergoes a two-step cooperative denaturation reaction, and the locations of two folding units have been deduced from NMR data. The SAXS technique provides complementary information on the size and shape of macromolecules, and it has been successfully applied to characterize non-native protein conformations (*17*, *18*). SAXS data show that the intermediate state, in which the N-terminal half is still folded but the C-terminal half is denatured, remains highly compact.

MATERIALS AND METHODS

Sample Preparation. Unlabeled OspA was expressed in *Escherichia coli* as described previously (*19*). For preparation of [^{15}N-Lys]-OspA, *E. coli* BL21 (DE3) cells containing the OspA expression vector were grown at 37 °C until OD_{600} reached ∼0.5. [α-^{15}N]-Lys (100 mg L^{-1}; Cambridge Isotope Labs) was added to the media, and then, after 30 min of incubation, protein expression was induced by an addition of isopropyl β-D-thiogalactopyranoside at a final concentration of 1 mM. The cells were harvested 3 h later by centrifugation. OspA was purified as previously described (*5*).

Differential Scanning Calorimetry. Calorimetric measurements were made with a Nano-DSC instrument (CSC, Utah) as described previously (*20*). Very small differences were found between data taken with 1 K/min and those with 0.5 K/min, indicating that the scanning rate dependence was small in this range of scanning rate (data not shown). Thus, a scanning rate of 1 K/min was used for further measurements. The protein concentrations were 2.49 and 2.42 mg mL^{-1} in sodium phosphate buffer (10 mM, pH 6.0) containing NaCl (50 mM) with and without GuHCl (0.4 M), respectively. The denaturation reaction was found to be reversible, since the trace of the rescanning of the same sample showed more than 80% agreement with that of the first scan.

Analysis of the DSC data was carried out by the use of a simplified version of a previously developed program (*21*) according to the following scheme

$$\mathrm{N} \Leftrightarrow \mathrm{I} \Leftrightarrow \mathrm{D}$$

where N, I, and D denote a native state, an intermediate state, and a denatured state, respectively.

Fluorescence Spectroscopy. GuHCl-induced equilibrium unfolding and refolding reactions were followed by measuring Trp fluorescence. Experiments were performed on a Spectronic AB-2 spectrofluorometer equipped with a motor-driven syringe. The cuvette temperature was kept at 30 °C. An unfolding experiment started with a 1.5 mL solution containing 5 μM OspA in sodium phosphate buffer (10 mM, pH 6.0) and NaCl (50 mM). An emission spectrum (300−400 nm; excitation at 290 nm) was recorded following an equilibration delay (5 min) after each injection (50 or 100 μL) of the buffer solution containing 5 μM OspA and GuHCl. A refolding experiment was performed by titrating GuHCl-denatured OspA with the buffer containing OspA. Unfolding curves were fit with a two-state model using a nonlinear least-squares routine (*22*, *23*) in the program Igor Pro (Wavemetrix, OR) on a Macintosh computer.

NMR Spectroscopy. All experiments were performed on a Varian Unity INOVA 600 spectrometer. The HSQC experiment was performed using a published procedure (*24*, *25*). For temperature-scanning experiments, data acquisition (∼4 h) was initiated after a temperature equilibration delay of 1 h. The protein concentration was approximately 0.3 mM in sodium phosphate buffer (10 mM, pH 6.0) containing NaCl (50 mM) and GuHCl (0.4 M) prepared in 95% H_2O/5% ^2H_2O. NMR spectra were processed with the NMRPipe suite (*26*) and analyzed with the NMRView program (*27*).

Analysis of Thermal Denaturation Data. Thermal denaturation data were analyzed by fitting the two-state model, based on the Gibbs-Helmholz equation and the linear baseline assumption, to the averaged peak intensities using a nonlinear least-squares routine (reviewed in ref *28*). Equations

$$K(T) = \frac{I_{\mathrm{N}}(T) - I(T)}{I(T)} = \exp([(\Delta H_{\mathrm{m}}(1 - T/T_{\mathrm{m}}) - \Delta C_{\mathrm{p}}\{\mathrm{T}_m - T + T\ln(T/T_{\mathrm{m}})\}]/-RT)$$

and

$$I_N(T) = I_N^{\ 0} + m_N T$$

were used in the fitting procedure, where $I_N(T)$ and $I(T)$ are the peak intensity for the native state at the temperature T and the measured intensity at T, respectively; I_N^0 is the intensity for the native state at $T = 0$, and m_N is the slope of $I_N(T)$ with respect to T; $K(T)$ is the equilibrium constant at T between the native and denatured states; T_m is the midpoint of the thermal denaturation curve, and ΔH_m is the enthalpy change upon denaturation at $T = T_m$; ΔC_P is the change in heat capacity between the native and denatured states. ΔC_P values for the N-terminal (residues 16−118) and C-terminal (residues 119−273) folding units were estimated according to the method of Myers et al. (*29*): $\Delta C_P \approx 172 + 17.6N$ (in cal mol^{-1} K^{-1}), where N is the number of residues. See Discussion for the choice of the boundary between the folding units.

SAXS Measurements and Data Analysis. The SAXS instrument and SAXS experiment method were as described before (*30*). The X-ray source is a Rigaku-RU 300 rotating-anode generator with a copper target producing 1.54 Å X-rays. The generator was operated at 9 kW. The detector is a two-dimensional multiwire detector with 256 × 144 pixels and a sensitive area of 290 × 288 mm^2. The X-ray beam was circularly collimated. No desmearing of the scattering data was necessary as shown by comparing the scattering data of a protein standard, bovine serum albumin, with and without taking account of the beam profile. The sample-to-detector distance could be changed between 1.4 and 2.3 m. This enabled an effective Q range of 0.01−0.60 Å^{-1} to be measured where $Q = 4\pi \sin\theta/\lambda$ is the magnitude of the scattering vector, 2θ is the scattering angle, and λ = 1.54 Å was the wavelength of the X-rays. Both the collimator and the sample-to-detector path were helium flushed. The sample cell was a 2 mm quartz capillary tube. The sample holder was temperature-controlled with a circulating water bath. SAXS measurements were from 28 to 61 °C. Samples were sealed with mineral oil to prevent evaporation.

The protein was buffer-exchanged to the 10 mM sodium phosphate, 50 mM NaCl, 0.1 mM EDTA, and 0.4 M GuHCl using a small Sephadex G25 column (Pharmacia NAP-5) after repeatedly concentrating and diluting the buffer with a Centricon-10. The same batch of buffer was used for SAXS background subtraction.

The radius of gyration was obtained by Guinier approximation (*31*):

$$\ln I(Q) = \ln I(0) - {}^1/_3 Q^2 Rg^2$$

in the QRg ≤ 1 region with a linear least-squares fitting routine. Two protein concentrations (10.5 and 5.25 mg/mL) were measured at each temperature. No concentration dependence of the radii of gyration was observed at these two concentrations at all temperatures measured, indicating that the intermolecular interaction effect is negligible. The $P(r)$ functions were generated from the scattering data by the GNOM program (*32*).

Singular value decomposition (SVD) analysis was performed by a FORTRAN program written on the basis of the SVD algorithm by Press et al. (*33*). A set of background subtracted $I(Q)$ curves, in a range of thermal denaturation temperatures, was arranged into an $M \times N$ matrix A whose number of rows M represents the number of Q points (M = 110 when 0.015 ≤ Q ≤ 0.24 Å^{-1}) and the number of columns N represents the number of temperatures measured (N = 11 from 28.4 to 60.9 °C). The matrix A can be decomposed into

$$A = UWV^{\mathrm{T}} \tag{1a}$$

where U is an $M \times N$ column-orthogonal matrix, W is an $N \times N$ diagonal matrix, and V^{T} is the transpose of an $N \times N$ orthogonal matrix. Equation 1a can also be written as a sum of outer products of columns of U and rows of V^{T}, with the weighting factors being the singular values w_j

$$A_{ij} = \sum_{k=1}^{N} w_k U_{ik} V_{jk} \tag{1b}$$

In cases when most of the singular values w_j of matrix A are very small, the matrix A can be approximated with only a few columns of U and V (the same k ones) with good accuracy. The minimum value of k represents the minimum number of components to reconstruct a scattering curve at the jth temperature

$$I_{jc}(Q) = \sum_{k=1}^{L} w_k U_{ik} V_{jk} \tag{2}$$

The minimum value of k, L, was determined by examining the singular values w_k; the random distribution of the normalized residues between the measured $I_j(Q_i)$ and the reconstructed $I_{j,cal}(Q_i)$, $r_j(Q_i) = (I_{j,cal}(Q_i) - I_j(Q_i))/\sigma_j(Q_i)$, where $\sigma_j(Q_i)$ is the error in $I_j(Q_i)$ derived from the counting statistics; and the global chi-square value

$$\chi^2 = \sum_{j=1}^{N}\sum_{i=1}^{M} \{r_j(Q_i)\}^2$$

RESULTS

DSC Measurements Reveal Two Separable Denaturation Transitions. DSC experiments were performed to characterize the thermodynamics of the equilibrium denaturation reaction of OspA. Figure 1A shows the DSC scan of OspA in sodium phosphate buffer (10 mM, pH 6.0) containing NaCl (50 mM), the same solvent conditions as those for our previous NMR studies (*5*). The DSC scan clearly shows two transition peaks, and the two components were curve-fitted well with a scheme, N ⇔ I ⇔ D, where N, I, and D denote the native state, an intermediate state, and a denatured state, respectively (Figure 1A). The thermodynamic parameters obtained from this analysis for the first step are the following: $t_{1/2}$, the temperature at which the reaction is half-complete, is 59.4 °C; and ΔH_{cal} (the calorimetric enthalpy at $t_{1/2}$) is 149 kcal mol^{-1}. Those for the second step are $t_{1/2}$ = 67.8 °C and ΔH_{cal} = 108 kcal mol^{-1}. These results demonstrate that the thermal denaturation reaction of OspA involves at least two cooperative transitions.

We then tried to characterize structural features of the thermal unfolding reaction of OspA using NMR spectroscopy. However, the transition temperature was too high for our NMR instrument. In addition, at a higher protein concentration required for NMR measurements, OspA precipitated at ~60 °C.

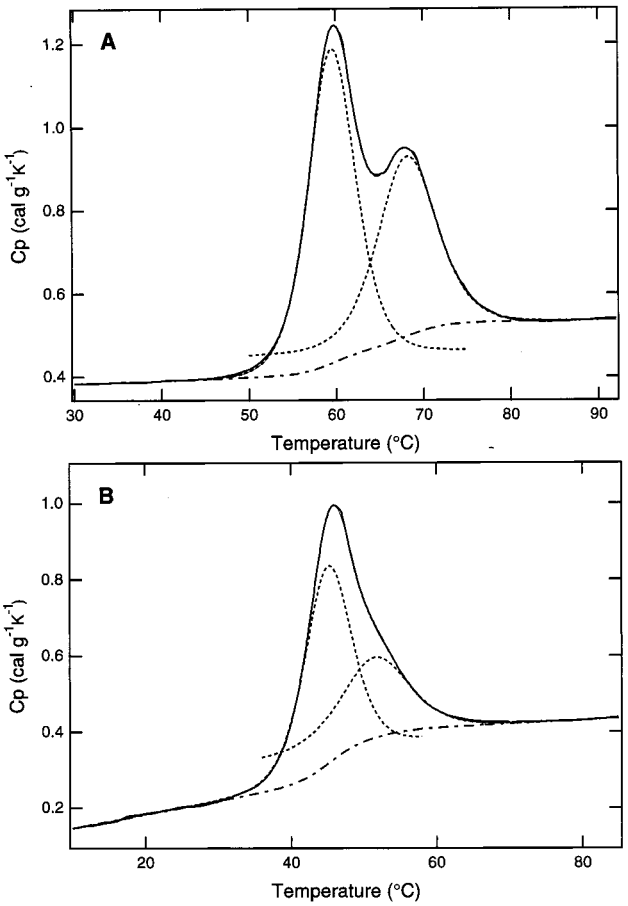

FIGURE 1: DSC measurements of OspA at pH 6.0 in the absence (A) and presence (B) of 0.4 M GuHCl. The solid lines represent experimental data. Data were fit with a scheme N ⇔ I ⇔ D, where N, I, and D denote the folded, intermediate, and fully denatured states. The best fit is shown as thin solid lines which almost completely coincide with the experimental data. Dashed lines show the resuting deconvoluted curves for two denaturation transitions. Dot-and-dash curves show the calculated baselines.

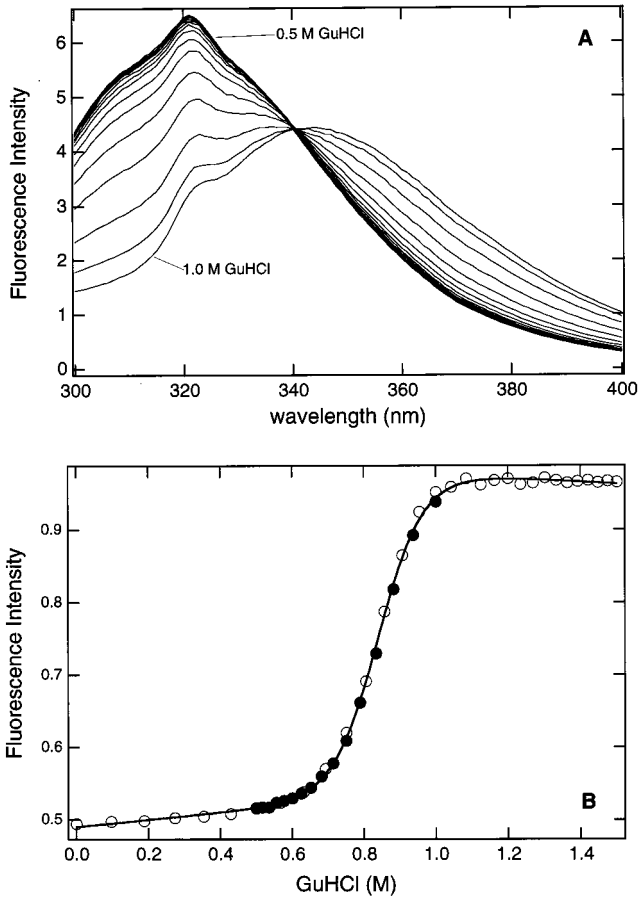

FIGURE 2: Denaturation of OspA monitored by Trp fluorescence. (A) Representative emission spectra of OspA in the transition region. (B) the fluorescence intensity plotted versus GuHCl concentration. The fluorescence intensity at 360 nm was normalized to that at 340 nm. The open circles indicate an unfolding transition, and the closed circles indicate a refolding transition. From curve fitting of the two-state model to the unfolding transition, the free energy of unfolding in the absence of GuHCl was determined to be 8.0 (±0.2, standard deviation) kcal mol^{-1} and the dependence of the free energy on GuHCl concentration was 9.5 (±0.2) kcal mol^{-1} M^{-1}.

To decrease the transition temperature and possibly eliminate protein precipitation by an addition of GuHCl, we characterized GuHCl-induced unfolding of OspA at 30 °C. Figure 2 shows the unfolding transition followed by fluorescence emission from the single Trp in the C-terminal domain. The unfolding reaction was almost fully reversible. The presence of an iso-fluorescent point at 340 nm in the spectra (Figure 1A) suggests that the unfolding transition of the region around the Trp residue is a two-state process. From the unfolding curve, we decided to include 0.4 M GuHCl in further characterization of thermal unfolding.

The DSC scan in the presence of 0.4 M GuHCl still shows the two separable transitions (Figure 1B), though the separation between the two peaks is smaller than that in the absence of GuHCl. The thermodynamic parameters for the first step are the following: $t_{1/2}$ is 44.8 °C, and ΔH_{cal} (the calorimetric enthalpy) is 124 kcal mol^{-1}. Those for the second step are $t_{1/2} = 51.0$ °C and $\Delta H_{cal} = 72.6$ kcal mol^{-1}.

Locations of the Two Folding Units Identified by NMR Spectroscopy. Though far-UV CD and fluorescence spectroscopies are the most common methods used to probe conformational changes during protein denaturation (*34*), these techniques are not well-suited for probing the denaturation reaction of OspA. OspA is a predominantly β-sheet protein. CD spectroscopy is most sensitive to helical secondary structure. It has been shown that the CD spectra of β-sheets have significant variations between proteins and they are also sensitive to the packing geometry (*35*). In addition, it is a macroscopic technique, and one cannot assign an observed change in CD spectrum to a specific structural change without further experiments. A previous study showed that there is only a small change in the far-UV CD spectrum of OspA upon denaturation (*36*). OspA contains a single Trp residue at position 216 in the C-terminal domain. Thus, the fluorescence emission spectrum of OspA is dominated by this Trp residue, and it only gives information on local structural changes in the C-terminal domain. Because of these reasons, we decided to probe the denaturation reaction of OspA using NMR spectroscopy. NMR is sensitive to secondary structure and local packing. It has been successfully used to follow protein denaturation reactions (for examples, see refs *37*−*39*). We have already established the resonance assignments for OspA, and thus we can follow conformational changes at specific locations.

Though OspA is quite large by current standards for solution NMR, it gives an exceptionally good ^{1}H, ^{15}N−

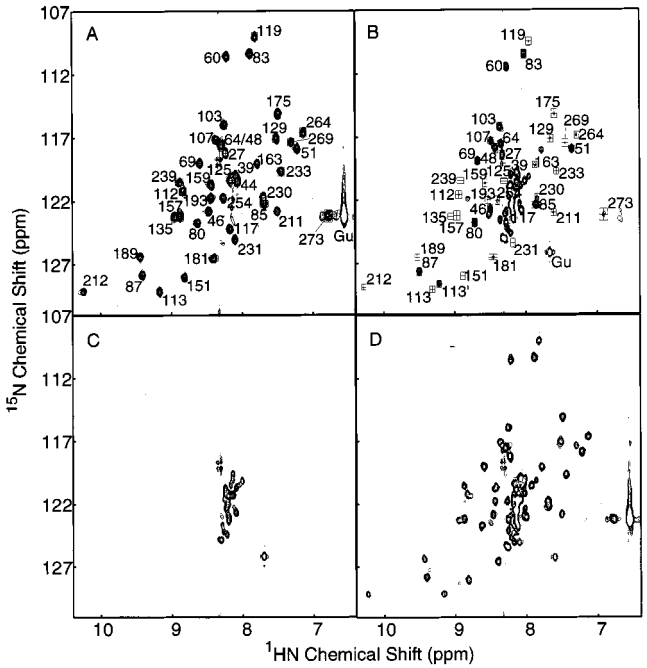

FIGURE 3: ^{1}H, ^{15}N-HSQC spectra of [^{15}N-Lys]-OspA in 0.4 M GuHCl at 30 (A), 45 (B), and 55 °C (C), and that of the same sample at 30 °C after cooling from 55 °C (D).

HSQC spectrum which correlates the chemical shift of directly attached ^{1}H and ^{15}N nuclei (*5*). We exploited this high-quality spectrum previously to obtain complete NMR assignments. However, the spectrum of the uniformly labeled protein is highly crowded with close to 300 cross-peaks, and it was difficult to follow the migration and intensity changes of peaks as the temperature was changed. To simplify the NMR spectrum while conserving as much information content as possible, we prepared an OspA sample which was specifically ^{15}N-labeled at the backbone amide nitrogen of Lys residues. This method has been successfully used to study apomyoglobin (*40*). OspA contains 40 Lys residues which are quite uniformly distributed throughout the molecule.

The HSQC spectra were collected on a [^{15}N-Lys]-OspA in the presence of 0.4 M GuHCl from 30 to 55 °C at 2.5 °C intervals. The temperature was then decreased to 30 °C. Figure 3 shows representative spectra. The cross-peaks in the spectrum collected at 30 °C were first assigned on the basis of our previous assignments (*5*). The peak positions in this spectrum are in an excellent agreement with those predicted from the assignments for the native protein, clearly indicating that OspA is fully folded under these conditions. The cross-peaks are well-separated in the spectrum, making it easy to follow the decay of peaks for the native state and the appearance of new peaks as the temperature was raised. The spectrum at 55 °C (Figure 3C) only contains cross-peaks clustering near $^{1}H = 8.5$ ppm, consistent with a spectrum of an unfolded protein. The spectrum collected at 30 °C after refolding (Figure 3D) has all of the cross-peaks that are present in the original 30 °C spectrum. The intensities of these peaks in the spectrum of the refolded protein were ~80% of those in the original spectrum, indicating that the refolding reaction was highly reversible even at a high protein concentration used for this experiment (9 mg mL^{-1}). There are additional peaks near the center of the spectrum, which suggest the presence of denatured or misfolded species. No sign of protein precipitation of OspA was found in the sample throughout data collection.

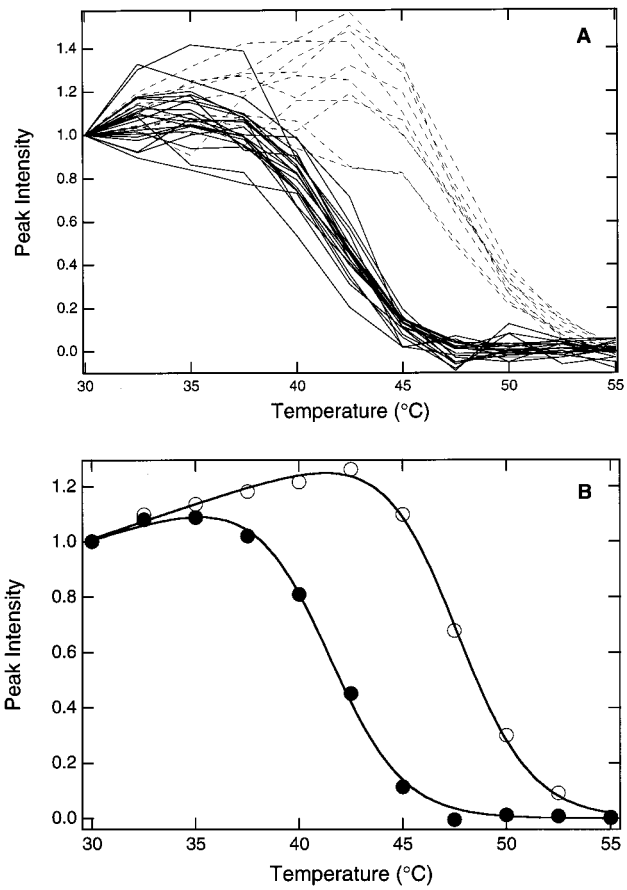

FIGURE 4: (A) Intensities of individual HSQC cross-peaks plotted versus temperature. Peak intensities are normalized to those at 30 °C. The continuous lines with a midpoint temperature of ~41 °C are for 21 residues located between positions 109 and 273. The dashed lines with a midpoint temperature of ~47 °C are for 10 residues located between positions 46 and 107. Residues 112 and 113 are not included in this plot (see text and Figure 6). (B) The average intensities of the 10 and 21 resonances in the N- and C-terminal folding units, shown with open circles and closed circles, respectively. The curves are the best fits of the data to the two-state denaturation model.

Of the 40 Lys residues in OspA we found that 32 residues could be used as conformational probes. Residues 27, 39, 44, 48, 64, 117, and 125 were excluded from analysis due to peak overlaps, and residue 18 was not detected due to rapid exchange of its amide proton with solvent. The temperature dependence of the intensity of each cross-peak is shown in Figure 4A. This figure clearly shows that the cross-peaks can be categorized into two groups in terms of temperature dependence of peak intensity. The first group shows a cooperative transition with a midpoint at approximately 41 °C, while the second group has a midpoint at approximately 47.5 °C. The first group with the lower transition temperature includes residues 119, 129, 135, 151, 157, 159, 163, 175, 181, 189, 193, 211, 212, 230, 231, 233, 239, 254, 264, 269, and 273. These residues are located in the last two strands of the central β-sheet and in the C-terminal domain (Figure 5). The second group includes residues 46, 51, 60, 69, 80, 83, 85, 87, 103, and 107. These are located in the N-terminal domain (Figure 5). The spectrum taken at 45 °C (Figure 3B) clearly shows this

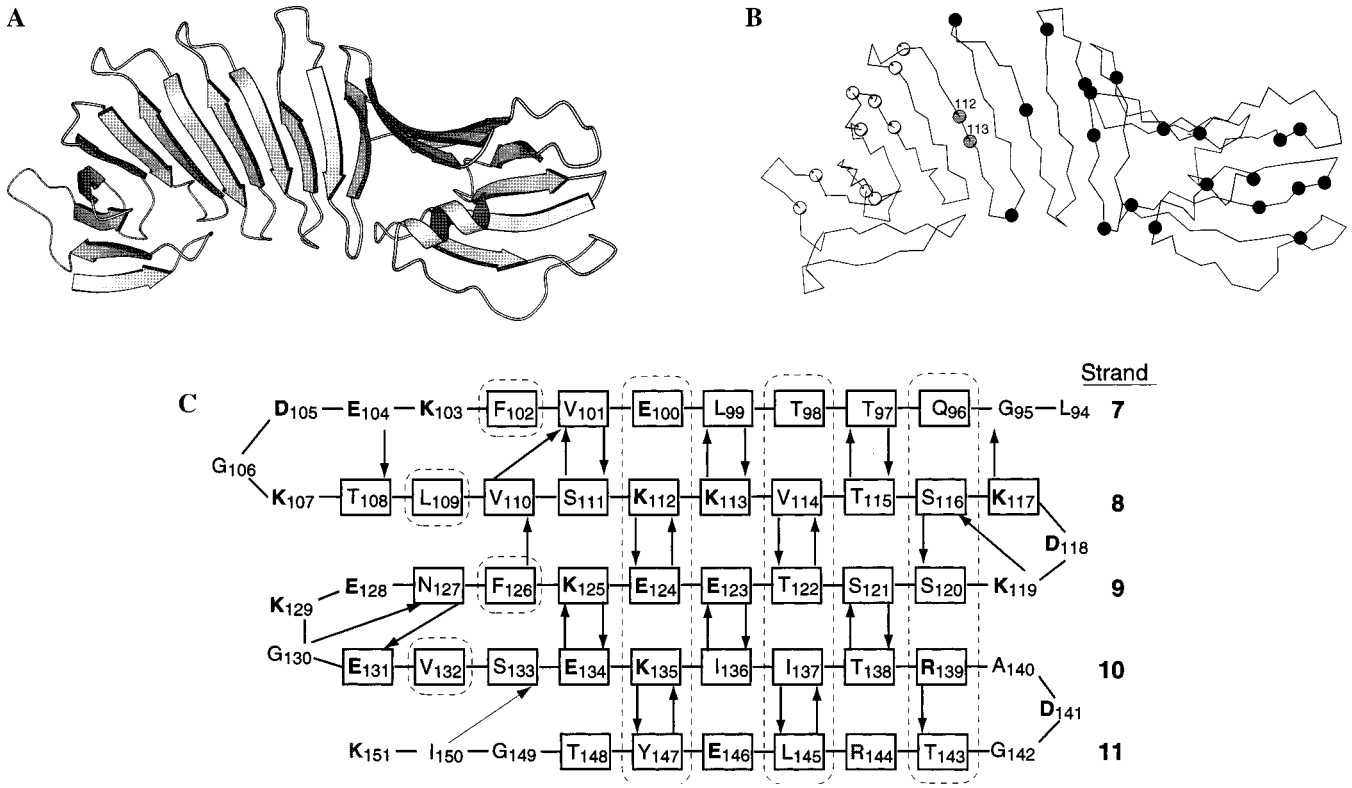

FIGURE 5: (A) Schematic drawing of OspA structure. (B) Lys residues in OspA. A black circle shows the position of a Lys residue which unfolds with a midpoint temperature of ~41 °C. A white circle shows a position that unfolds with a midpoint temperature of ~47 °C. Lys residues that are excluded from analysis due to peak overlap are not shown. Residues 112 and 113 are shown as gray circles and labeled with a residue number. (C) Schematic drawing of the central β-sheet of OspA. Residues enclosed with rectangles are those within β-strands. Hydrogen bonds are shown as arrows with the arrowheads pointing to the carbonyl groups. Residues enclosed in dashed lines have side chains protruding toward the reader. Panels A and B were made with MOLSCRIPT (*57*).

distinction between the two groups of cross-peaks. The first group has weak peaks in the spectrum, while the second group retains strong peaks. These results indicate that the C-terminal globular domain and the last two strands of the central β-sheet (residues 119−273) denature before the N-terminal globular domain (residues 16−107) denatures.

The cross-peak for residue 113 in the central β-sheet exhibited an unusual pattern of temperature dependence. The intensity of the original peak for this residue decreased following the first transition. However, we observed concomitant appearance of a cross-peak in the vicinity of the original peak (Figure 6). The intensity of the "daughter" peak increases with the same temperature dependence as the denaturation of the C-terminal folding unit, and it decays with the second transition. We tried to assign this new peak using the magnetization transfer technique at the midpoint of the first transition. However, no cross-peaks were observed for this peak in a ^{15}N-double edited NOESY experiment due to an amide hydrogen exchange rate that was significantly faster than the interconversion rate between the native and the intermediate states (data not shown). Though we could not establish an unambiguous assignment for this daughter peak, its proximity to the cross-peak for residue 113 in a well-isolated region of the spectrum strongly suggests that this daughter peak belongs to residue 113. Further, the sum of peak intensities for residue 113 and its daughter peak closely follows the average transition curve for the N-terminal residues (Figure 6B). In the OspA structure there are two Lys residues in the vicinity of Lys 113. The peak

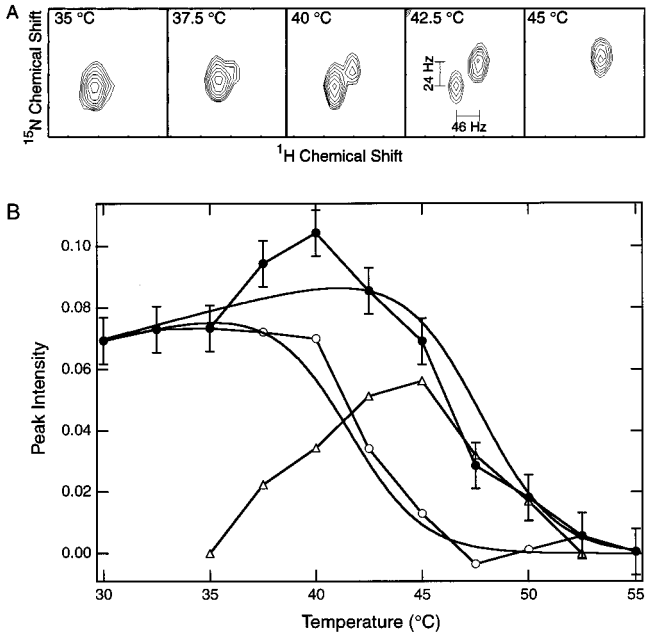

FIGURE 6: (A) Appearance of new peaks for residue 113. Sections of HSQC spectra which include the original and new peaks for the residue are shown. (B) Peak intensities of residue 113 plotted as a function of temperature. Open circles indicate the intensity of the original peak; triangles, that of the new peak; and closed circles, the sum of the two peak intensities. Errors were estimated from noise in the spectra and are shown only for the total peak intensity for clarity. The two curves show the denaturation curves of the two folding units as determined in Figure 4B.

intensity for residue 112 follows the first transition. We also observed an appearance of a new peak in its vicinity. However these cross-peaks are located in a crowded region close to the center of the spectrum, and we could not make a strong argument about the identity of the new peak. The cross-peak for residue 119 is well-isolated (Figure 3). This cross-peak decays with the other peaks in the C-terminal folding unit, and we did not observe a new peak in the neighborhood of this cross-peak.

We did not observe large changes in the line shape of cross-peaks as OspA denatured. This observation indicates that the respective interconversion rates between the fully folded and intermediate states and between the intermediate and fully denatured states are slow relative to the corresponding chemical shift differences of cross-peaks. From the cross-peaks for residue 113, we can estimate the upper limit of these interconversion rates to be 20−50 Hz.

NMR data were then used to estimate stabilities of the two folding units in OspA. As the temperature is increased and thus the molecular tumbling rate increases, the NMR line shape becomes sharper. Concomitantly, the exchange rate for an amide proton with the solvent becomes faster. Therefore, we do not expect the peak intensities to remain constant in the thermal denaturation experiment, even in the temperature range where no conformational transition occurs. Rather, they should be a complex function of temperature. However, in practice, the average intensity for the N-terminal unit has a quite linear dependence on temperature in the region where the unit is predominantly folded (30−40 °C). Therefore, we analyzed these thermal denaturation curves according to the standard two-state model and the linear baseline approximation for the native and denatured states. Because a cross-peak shifts drastically upon denaturation so that the denatured state does not have a cross-peak at the same position as the native state, the peak intensity for a cross-peak in the denatured state was taken to be zero. The C-terminal unit does not have a sufficient baseline region for the native state. We assumed that the native baseline for the C-terminal unit has the same slope as that for the N-terminal unit. This assumption is reasonable because there is no qualitative difference in distribution of Lys residues in the two folding units (see Figure 5). The midpoints of the thermal denaturation curves were determined to be 47.3 (± 0.2) and 41.1 (± 0.1) °C for the N- and C-terminal folding units, respectively. The enthalpy changes at the transition midpoint, ΔH_m, were 111 and 105 kcal mol^{-1} for the N- and C-terminal folding units, respectively. The difference in the free energy between the two units, $\Delta\Delta G_0$, at the transition midpoint for the C-terminal unit (41.1 °C) was 2.0 kcal mol^{-1}. These thermodynamic parameters are in a reasonable agreement with those determined with DSC (see above). The midpoints of the two transitions derived from the NMR data are 3.7 °C lower than their respective values from the DSC experiments. These differences may be attributed to differences in protein concentration, temperature-scanning rate, and sample preparation (see below). The unfolding standard free energy, ΔG_0, of the C-terminal folding unit at 30 °C in the presence of 0.4 M GuHCl was estimated to be 3.2 kcal mol^{-1} from the NMR data. This value is in a reasonable agreement with the corresponding value determined from the fluorescence experiment (4.2 kcal mol^{-1}), and that from the DSC data (5.2 kcal mol^{-1}).

Global Structural Changes Revealed by SAXS Measurements. We then used SAXS to probe the overall conformation of OspA. From the slope of a plot of ln $I(Q)$ vs Q^2, one can determine the electronic radius of gyration (Rg) (*17*, *41*). Rg is extremely sensitive to the spatial extent of a particle. Figure 7A shows the Guinier plot of OspA at different temperatures. There is a small (∼10%) increase in Rg as the temperature was raised from 28.4 to 41.5 °C (Figure 7B). As the temperature was further raised, a dramatic increase in Rg was observed. At 60.4 °C, Rg was determined to be 56.1 ± 1.6 Å, which is close to the Rg value (60 Å) calculated for the random coil state of OspA (*42*). The forward scattering intensity $I(0)$, which is sensitive to the molecular weight of the scatterer, remained unchanged (Figure 7A), demonstrating the absence of protein aggregation upon thermal denaturation in the temperature range measured by SAXS.

From the entire scattering curves collected at both small and larger angles, one can obtain information regarding the overall shape of the particle (*17*, *41*). A Fourier inversion of scattered intensity gives a radial Patterson ($P(r)$) curve that is a real-space representation of the information in a scattering curve. A $P(r)$ curve shows the length distribution of atom-weighted interatomic vectors in the particle. The $P(r)$ curve of OspA at 30 °C closely matches the $P(r)$ curve calculated from the crystal structure with a maximum molecular dimension of about 85 Å (*6*). At 41.5 °C, the $P(r)$ curve of OspA has an average maximum molecular dimension of about 110 Å (Figure 7C). As the temperature was further increased, the protein became significantly more expanded. At the highest temperature, the protein is highly extended, with the average maximum molecular dimension length approximately 3 times longer than that of the folded protein.

The $P(r)$ curves at different temperatures have two apparent iso-crossing points (see Figure 7C), suggesting that the thermal denaturation of OspA may not be a two-state process. Thus, the scattering data were also analyzed by the singular value decomposition (SVD) method. The SVD method has been applied to SAXS studies of quaternary structure change and protein unfolding problems (*43*−*46*). SVD analysis is capable of determining the minimum number of species present in the sample to account for the scattering data within experimental error, without a prior knowledge of the structural information of the individual species. However, it should be emphasized that, although SVD can determine the minimum number of species in the scattering data, the significant basis functions used to reconstruct the scattering curve do not represent the scattering curves of particular molecular species (*44*). Based on the χ^2 (see Figure 6D) and the random fluctuations of the normalized residues between −1 and +1, SVD analysis demonstrates that the denaturation of OspA contained three distinct species, consistent with the results of the DSC and NMR measurements.

For an ensemble mixture of macromolecules of the same molecular weight but of different sizes, the scattering intensity $I(Q)$ and the Rg^2 are number averaged values. The $I(Q)$ and the Rg^2 observed for a mixture of three conformational states can be expressed as

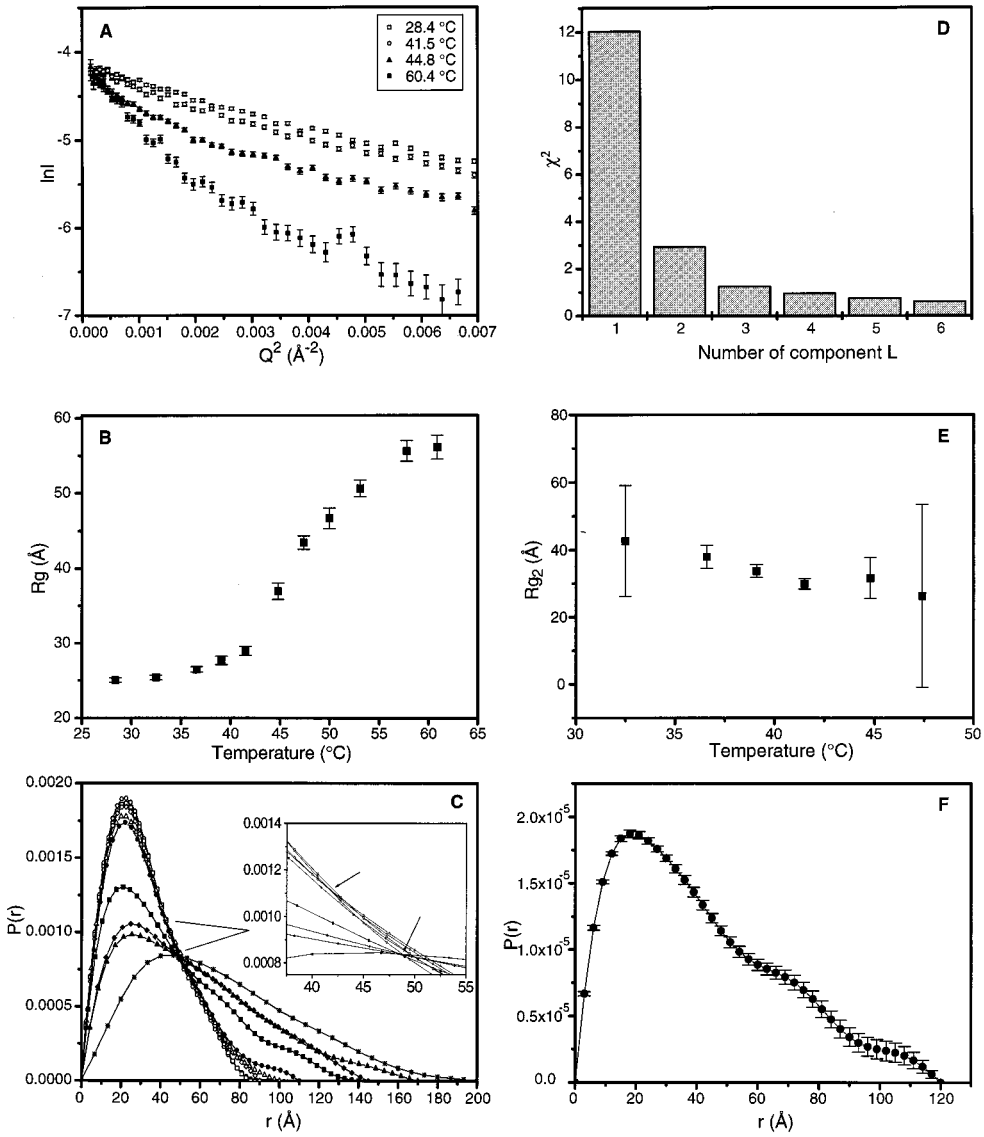

FIGURE 7: (A) The Guinier plot of SAXS data recorded at 28.4, 41.5, 44.8, and 60.4 °C. (B) The radius of gyration, Rg, determined from the SAXS data plotted as a function of temperature. (C) The $P(r)$ plot of OspA in 0.4 M GuHCl at various temperatures (from top to bottom in the small r region, 28.4, 32.5, 36.6, 39.1, 41.5, 44.8, 47.4, 50.0, and 60.4 °C). There are two apparent iso-crossing points in the $P(r)$ functions (see the inset). (D) The global χ^2 of the SVD analysis of the scattering data plotted as a function of the number of species L. With $L = 3$, χ^2 becomes close to 1, suggesting that the thermal denaturation of OspA has a minimum number of three components. When $L > 3$, χ^2 is further reduced but the small decrease does not necessarily mean a better fit of the reconstructed SVD curve to the experimental data since χ^2 is less than 1. (E) The radius of gyration of the intermediate, Rg_2, plotted as a function of temperature. (F) The $P(r)$ function of the intermediate state calculated from eq 3a on the basis of the number of fractions estimated from the NMR data.

$$I(Q) = x_1 I(Q)_1 + x_2 I(Q)_2 + x_3 I(Q)_3 \qquad (3a)$$

$$\mathrm{Rg}^2 = x_1 \mathrm{Rg}_1{}^2 + x_2 \mathrm{Rg}_2{}^2 + x_3 \mathrm{Rg}_3{}^2 \qquad (3b)$$

where x is the number fraction of a molecular species and subscripts 1, 2, and 3 denote the folded, intermediate, and unfolded states, respectively. These number fractions can be calculated on the basis of a two-step denaturation model using the equilibrium constants of denaturation, K_1 (for the C-terminal folding unit) and K_2 (for the N-terminal folding unit), from the NMR thermal denaturation data

$$x_1 = \frac{1}{1 + K_1 + K_1K_2}, \quad x_2 = \frac{K_1}{1 + K_1 + K_1K_2},$$

$$\text{and } x_3 = \frac{K_1K_2}{1 + K_1 + K_1K_2}$$

We chose to use the equilibrium constants from the NMR data, rather than those from the DSC measurements, because of the following reasons. There may have been a small systematic difference in GuHCl concentration between the DSC samples and the NMR and SAXS samples. The NMR and SAXS samples were both prepared at University of Rochester, while the DSC samples were prepared at Kobe University. Also the protein concentration and the measurement time per temperature point used in the SAXS experiments were quite similar to those in the NMR experiment, but a lower protein concentration and significantly faster temperature-scanning rates were used in the DSC measurements. It was not possible to record interpretable DSC data with a temperature-scanning rate similar to those employed in the NMR and SAXS experiments. This is because DSC measurements require a faster rate for sensitivity.

In this calculation, Rg values measured at 28.4 and 61.0 °C were used as Rg_1 and Rg_3, respectively. The value for Rg_2 remained unchanged within error in the transition region of 35−50 °C in which the intermediate state is most populated (Figure 7D). This suggested that the thermal denaturation of OspA could indeed be considered as a three-state unfolding process comprising two transitions as revealed by the DSC and NMR experiments. The averaged Rg_2 in the 35−50 °C was determined to be 33 ± 4 Å. The $P(r)$ function of the intermediate state was also calculated from $I(Q)_2$ based on eq 3a (Figure 7F). The radius of gyration of the intermediate state calculated from this $P(r)$ function was 34.4 ± 1.0 Å.

DISCUSSION

We have shown that the denaturation reaction of OspA at equilibrium involves two separate transitions, and that the intermediate state contains the N-terminal folding unit in the folded form and the C-terminal folding unit in the denatured form. The SAXS data indicate that this intermediate is compact with a radius of gyration approximately 1.3 times larger than the fully folded protein. Upon denaturation of the N-terminal folding unit, the protein significantly expands to a more random coil-like state.

Our data clearly show the two distinct cooperative transitions in the denaturation reaction of OspA, and from the NMR data it is clear that the boundary between the two folding units is located within the central β-sheet (Figure 5). However, the exact boundary has not yet been precisely defined. There are eight Lys residues in the central β-sheet (strands 8−10; Figure 5C). Unfortunately residues 117 and 125, which lie at critical positions, had to be excluded from analysis due to peak overlap. Residues 119, 129, and 135 were categorized with the C-terminal folding unit. In contrast, residue 113 seems to be a part of the N-terminal unit. Though the original peak for residue 113 decays concomitantly with the denaturation of the C-terminal folding unit, a new peak appears in the vicinity of the original peak (Figure 6). These observations suggest that residue 113 is still folded as the C-terminal folding unit denatures, but its resonance frequencies are affected by the denaturation of nearby residues. The peak intensity for residue 112 follows the transition for the C-terminal unit, and a new peak concomitantly appears in its vicinity, suggesting that the peak for residue 112 is also affected by denaturation of the C-terminal domain. As described above, our attempts to assign these new peaks using the magnetization transfer method were not successful, because of the rapid amide hydrogen exchange rates at the relatively high temperature used (41.5 °C). This technique was successfully used for other systems under more favorable conditions (for example, see ref *47*). Thus, the assignments of these new peaks are still tentative, particularly for residue 112 which is in a crowded region. It is also possible that the peak for residue 112 shifts drastically upon denaturation of the C-terminal unit. The amide proton of Lys 112 is hydrogen bonded to Glu 124 (Figure 5C), and thus denaturation of the C-terminal folding unit is expected to cause a large shift of the Lys 112 resonance. In contrast, the amide proton of Lys 113 is hydrogen-bonded to Leu 99 in the N-terminal fragment (Figure 5C), and denaturation of the C-terminal unit should not cause a large shift of this amide proton. Taken together, these results suggest that strand 8 which includes residues 112 and 113 belongs to the N-terminal folding unit, and strands 9 and 10 are included in the C-terminal unit. The boundary between the two folding units may be better defined by performing unfolding experiments using OspA samples which are ^{15}N-labeled at positions other than Lys residues.

The results from this study are consistent with previous results on OspA. Amide H−D exchange experiments indicate that the N-terminal folding unit (strands 1−8) has the highest protection and that strands 9−11 have intermediate protection (*7*). The remaining C-terminal segment has the least protection, but the most protected residue (residue 230) has a protection comparable to those for residues in strands 9−11. It has been shown that in small globular proteins, the free energy derived from the most protected amide proton closely agrees with the global stability determined by equilibrium unfolding (*48*). The consistency between the H−D exchange data and the results in this study suggests that amide exchange experiments can predict stability differences among folding units in a protein. It should be noted that the two folding units of OspA have few interactions, and that this situation is quite different from folding units within a globular protein.

Huang et al. showed that a C-terminal fragment corresponding to residues 130−273 has a significantly decreased conformational stability compared to the full-length protein (Huang, X., Dunn, J. J., Lawson, C. L., Luft, B. J., and Koide, S., unpublished results). They found that the *m* value, that is, the dependence of the free energy on denaturant concentration, for the C-terminal fragment, as monitored by fluorescence from the single Trp, is nearly identical to that of the full-length protein. The *m* value has been shown to correlate well with the change in the solvent-accessible surface area upon denaturation (*29*). Therefore, the similar *m* values suggested that similar changes in the solvent-accessible surface area accompany the denaturation reaction of the C-terminal segment within full-length OspA and in the C-terminal fragment. This, in turn, suggests that the C-terminal segment is an independent folding unit.

Though the equilibrium denaturation reaction does not necessarily correspond to the kinetic folding reaction, the two-step denaturation mechanism of OspA demonstrated in this study and the low stability of a C-terminal fragment suggest that the N-terminal folding unit may serve as a template upon which the C-terminal folding unit is assembled. Interactions within the single-layer β-sheet might then couple the high stability of the N-terminal unit to the C-terminal unit. Pham et al. proposed that hydrophobic clusters and long side chains of Glu and Lys are the major factors for the high stability of the single-layer β-sheet (*7*). Cross-strand electrostatic interactions between the characteristic Glu-Lys pairs (Figure 5C) may also contribute to stability. It will be interesting to see how mutations in this segment affect stability of the two folding units.

The C-terminal domain of OspA is the target of protective antibodies (*15, 16*). It also contains hypervariable regions which have been identified from a sequence analysis (*49*). Thus, it is intriguing that OspA has the more stable N-terminal domain that is highly conserved and possibly acts as a folding template for the hypervariable C-terminal domain. This architecture might be evolutionally advantageous, because the stabilization by the N-terminal domain

allows mutations in the C-terminal domain which may destabilize the protein but helps to change OspA's immunogenicity, thereby evading recognition by the immune system. Our findings have significant implications for the design of a Lyme disease vaccine based on OspA fragments. Protective anti-OspA antibodies bind to conformational epitopes in the C-terminal domain. The N-terminal domain contains a region which has shown to elicit unwanted side effects (*50*). Thus, a vaccine based on the C-terminal domain is desired. An OspA fragment used as a vaccine needs to be folded in order to elicit antibodies that recognize conformational epitopes in the folded form of OspA. The folding mechanism of OspA implicated by our data suggests that the removal of the N-terminal domain would always significantly decrease the conformational stability. A new strategy is required to compensate this loss of stability, to engineer a vaccine based on a C-terminal fragment of OspA.

The intermediate state of OspA found in this study is highly compact. However, available data suggest that the denatured C-terminal folding unit in this state does not correspond to the classical definition of the molten globule state. We use the term "molten globule" as a state in which a protein has nativelike secondary structure but lacks specific tertiary contacts (*51*, *52*). In contrast to the molten globule state of apomyoglobin, which exhibits a number of cross-peaks which are shifted from the random coil chemical shift (*53*), the HSQC peaks for the denatured state of the OspA C-terminal unit are all clustered near the random coil shift (Figure 2B). Also the time scale of the interconversion between the fully folded state and the intermediate state is slow compared to the chemical shift difference (20−50 Hz). This slow interconversion rate suggests that there is a significant energy barrier between the two states, which may correspond to a large structural rearrangement. The C-terminal folding unit in the intermediate may be best described as a collapsed denatured state which is stabilized by hydrophobic interactions (*54*, *55*).

The OspA intermediate contains the fully folded N-terminal folding unit. The OspA intermediate state appears to bear a strong resemblance to the so-called Shortle fragment of Staphylococcal nuclease. In this large fragment, the N-terminal β-sheet is largely retained, while the rest of the protein is disordered, as judged by NMR and calorimetry (*54*, *56*). Flanagan et al. showed, using SAXS, that this fragment is highly compact (*41*). It is intriguing to point out that the OspA intermediate and the Shortle fragment are both partially folded and compact. This may be simply because the conditions used to populate these partially folded states are not strong enough to induce highly denatured states. However, it is also possible that the folded domain provides a rigid surface to stabilize a compact state. These alterations can be tested in a comparison of the conformation of the C-terminal folding unit as an isolated fragment and that in the OspA intermediate under same conditions.

This study demonstrates that the use of heteronuclear NMR spectroscopy in conjunction with selective amino acid labeling provides a powerful means to monitor conformational changes at multiple positions in a protein. Selective labeling significantly simplifies the NMR spectrum and its analysis, while retaining a high degree of information content. This method may be particularly useful for distinguishing a partially folded protein containing a folded segment and an unfolded segment from a molten globule, which has nativelike secondary structure but lacks specific tertiary structure (*40*). It should be noted that most model proteins used in folding studies are smaller than OspA (28 kDa), so that the application of this technique to those proteins should be straightforward. Even in the absence of resonance assignments, these experiments would be quite useful in identifying multistep unfolding transitions.

The present characterization of the denaturation processes of OspA provides a basis for elucidating important interactions in its stability and folding mechanism. This protein contains at least two distinct folding units. The more stable N-terminal folding unit appears to act as a folding template for the C-terminal unit. The single-layer β-sheet part separating the globular domains is not itself a single folding unit. The interactions between the two folding units mediated by the single-layer β-sheet appear critical for stabilizing the C-terminal folding unit. Contributions of individual interactions in the central β-sheet to the stability of OspA are presently under investigation.

ACKNOWLEDGMENT

We are thankful to Dr. X. Huang for helpful discussions; Dr. D. Eliezer for helpful discussions and critical reading of the manuscript; Dr. S. D. Kennedy and A. Koide for technical assistance; and Prof. K. Akasaka for use of the DSC equipment. We also thank an anonymous reviewer for his/her constructive comments.

REFERENCES

1. Kauzmann, W. (1959) *Adv. Protein Chem. 14*, 1−63.
2. Dill, K. A. (1990) *Biochemistry 29*, 7133−7155.
3. Tanford, C. (1980) *The hydrophobic effect*, Wiley, New York.
4. Li, H., Dunn, J. J., Luft, B. J., and Lawson, C. L. (1997) *Proc. Natl. Acad. Sci. U.S.A. 94*, 3584−3589.
5. Pham, T. N., and Koide, S. (1998) *J. Biomol. NMR 11*, 407−414.
6. Bu, Z., Koide, S., and Engelman, D. M. (1998) *Protein Sci. 7*, 2681−2683.
7. Pham, T.-N., Koide, A., and Koide, S. (1998) *Nat. Struct. Biol. 5*, 115−119.
8. Smith, C. K., Withka, J. M., and Regan, L. (1994) *Biochemistry 33*, 5510−5517.
9. Smith, C. K., and Regan, L. (1995) *Science 270*, 980−982.
10. Minor, D. L. J., and Kim, P. S. (1994) *Nature 367*, 660−663.
11. Minor, D. L. J., and Kim, P. S. (1994) *Nature 371*, 264−267.
12. Otzen, D. E., and Fersht, A. R. (1995) *Biochemistry 34*, 5718−5724.
13. Ramirez-Alvarado, M., Blanco, F. J., and Serrano, L. (1996) *Nat. Struct. Biol. 3*, 604−612.
14. Fikrig, E., Barthold, S. W., Kantor, F. S., and Flavell, R. A. (1990) *Science 250*, 553−556.
15. Sears, J. E., Fikrig, E., Nakagawa, T. Y., Deponte, K., Marcantonio, N., Kantor, F. S., and Flavell, R. A. (1991) *J. Immunol. 147*, 1995−2000.
16. McGrath, B. C., Dunn, J. J., Gorgone, G., Luft, B. J., Guttman, D., and Dykhuizen, D. (1995) *Infect. Immunol. 63*, 1356−1361.
17. Lattman, E. E. (1994) *Curr. Opin. Struct. Biol. 4*, 87−92.
18. Kataoka, M., and Goto, Y. (1996) *Folding Des. 1*, R107−R114.
19. Dunn, J. J., Lade, B. N., and Barbour, A. G. (1990) *Protein Expression Purif. 1*, 159−168.
20. Tamura, A. (1998) *Thermochim. Acta 308*, 35−40.
21. Tamura, A., and Sturtevant, J. M. (1995) *J. Mol. Biol. 249*, 625−635.

22. Santoro, M. M., and Bolen, D. W. (1988) *Biochemistry 27*, 8063−8068.
23. Koide, S., Dyson, H. J., and Wright, P. E. (1993) *Biochemistry 32*, 12299−12310.
24. Kay, L. E., Keifer, P., and Saarinen, T. (1992) *J. Am. Chem. Soc. 114*, 10663−10665.
25. Grzesiek, S., and Bax, A. (1993) *J. Am. Chem. Soc. 115*, 12593−12594.
26. Delaglio, F., Grzesiek, S., Vuister, G. W., Zhu, G., Pfeifer, J., and Bax, A. (1995) *J. Biomol. NMR 6*, 277−293.
27. Johnson, B. A., and Blevins, R. A. (1994) *J. Biomol. NMR 4*, 603−614.
28. Pace, C. N., and Sholtz, J. M. (1997) in *Protein structure. A practical approach* (Creighton, T. E., Ed.) Vol. pp 299−321, IRL Press, Oxford, U.K.
29. Myers, J. K., Pace, C. N., and Scholtz, J. M. (1995) *Protein Sci. 4*, 2138−2148.
30. Bu, Z., Perlo, A., Johnson, J., Olack, J., Engelman, D. M., and Wyckoff, H. W. (1998) *J. Appl. Crystallogr.* (in press).
31. Glatter, O., and Kratky, O. (1982) *Small-angle X-ray scattering*, Academic Press, London, U.K.
32. Semenyuk, A. V., and Svergun, D. I. (1991) *J. Appl. Crystallogr. 24*, 537−540.
33. Press, W. H., Flannery, B. P., Teukolsky, S. A., and Vetterling, W. T. (1992) *Numerical Recipes*, Cambridge University Press, New York.
34. Schimid, F. X. (1997) in *Protein structure. A practical approach* (Creighton, T. E., Ed.) Vol. pp 261−298, IRL Press, Oxford, U.K.
35. Perczel, A., Park, K., and Fasman, G. D. (1992) *Proteins 13*, 57−69.
36. France, L. L., Kieleczawa, J., Dunn, J. J., Hind, G., and Sutherland, J. C. (1992) *Biochim. Biophys. Acta 1120*, 59−68.
37. Egan, D. A., Logan, T. M., Liang, H., Matayoshi, E., Fesik, S. W., and Holzman, T. F. (1993) *Biochemistry 32*, 1920−1927.
38. Frieden, C., Hoeltzli, S. D., and Ropson, I. J. (1993) *Protein Sci. 2*, 2007−2014.
39. Schulman, B. A., Kim, P. S., Dobson, C. M., and Redfield, C. (1997) *Nat. Struct. Biol. 4*, 630−634.
40. Eliezer, D., Jennings, P. A., Dyson, H. J., and Wright, P. E. (1997) *FEBS Lett. 417*, 92−96.
41. Flanagan, J. M., Kataoka, M., Shortle, D., and Engelman, D. M. (1992) *Proc. Natl. Acad. Sci. U.S.A. 89*, 748−752.
42. Miller, W. G., and Goebel, C. V. (1968) *Biochemistry 7*, 3925−3935.
43. Fetler, L., Tauc, P., Herve, G., Moody, M. F., and Vachette, P. (1995) *J. Mol. Biol. 251*, 243−255.
44. Chen, L., Hodgson, K. O., and Doniach, S. (1996) *J. Mol. Biol. 261*, 658−671.
45. Provencher, S. W., and Glockner, J. (1983) *J. Biochem. Biophys. Methods 7*, 331−334.
46. Segel, D. J., Fink, A. L., Hodgson, K. O., and Doniach, S. (1998) *Biochemistry 37*, 12443−12451.
47. Zhang, O., Kay, L. E., Olivier, J. P., and Forman-Kay, J. D. (1994) *J. Biomol. NMR 4*, 845−858.
48. Bai, Y., Milne, J. S., Mayne, L., and Englander, S. W. (1994) *Proteins 20*, 4−14.
49. France, L. L., Kieleczawa, J., Dunn, J. J., Luft, B. J., Hind, G., and Sutherland, J. C. (1993) *Biochim. Biophys. Acta 1202*, 287−296.
50. Kamradt, T., Lengl-Janssen, B., Strauss, A. F., Bansal, G., and Steer, A. C. (1996) *Infect. Immunol. 64*, 1284.
51. Ptitsyn, O. B. (1992) in *Protein Folding* (Creighton, T. E., Ed.) pp 243−300, Freeman, New York.
52. Kuwajima, K. (1989) *Proteins 6*, 87−103.
53. Eliezer, D., Yao, J., Dyson, H. J., and Wright, P. E. (1998) *Nat. Struct. Biol. 5*, 148−155.
54. Shortle, D., and Abeygunawardana, C. (1993) *Structure 1*, 121−134.
55. Lattman, E. E., Fiebig, K. M., and Dill, K. A. (1994) *Biochemistry 33*, 6158−6166.
56. Griko, Y. V., Gittis, A., Lattman, E. E., and Privalov, P. L. (1994) *J. Mol. Biol. 243*, 93−99.
57. Kraulis, P. (1991) *J. Appl. Crystallogr. 24*, 946−950.

BI982443+